

Magnetoelectric effect near spin reorientation transition in giant magnetostrictive-aluminum nitride thin film structure

Nicolas Tiercelin, A. Talbi, V. Preobrazhensky, P. Pernod, V. Mortet et al.

Citation: *Appl. Phys. Lett.* **93**, 162902 (2008); doi: 10.1063/1.3001601

View online: <http://dx.doi.org/10.1063/1.3001601>

View Table of Contents: <http://apl.aip.org/resource/1/APPLAB/v93/i16>

Published by the [American Institute of Physics](http://www.aip.org).

Related Articles

Design and optimization of voice coil actuator for six degree of freedom active vibration isolation system using Halbach magnet array

Rev. Sci. Instrum. **83**, 105117 (2012)

The tracking control system of the VLT Survey Telescope

Rev. Sci. Instrum. **83**, 094501 (2012)

Multi-functional dielectric elastomer artificial muscles for soft and smart machines

App. Phys. Rev. **2012**, 7 (2012)

Multi-functional dielectric elastomer artificial muscles for soft and smart machines

J. Appl. Phys. **112**, 041101 (2012)

Tactile feedback control for a gripper driven by SMA springs

AIP Advances **2**, 032134 (2012)

Additional information on Appl. Phys. Lett.

Journal Homepage: <http://apl.aip.org/>

Journal Information: http://apl.aip.org/about/about_the_journal

Top downloads: http://apl.aip.org/features/most_downloaded

Information for Authors: <http://apl.aip.org/authors>

ADVERTISEMENT



Goodfellow
metals • ceramics • polymers • composites
70,000 products
450 different materials
small quantities fast

www.goodfellowusa.com

Magnetoelectric effect near spin reorientation transition in giant magnetostrictive-aluminum nitride thin film structure

Nicolas Tiercelin,^{1,a)} A. Talbi,¹ V. Preobrazhensky,¹ P. Pernod,¹ V. Mortet,² K. Haenen,² and A. Soltani³

¹Joint European Laboratory LEMAC, IEMN, CNRS 8520, Ecole Centrale de Lille, Villeneuve d'Ascq 59651, France

²IMO, Limburgs Universitair Centrum, Wetenschapspark 1, 3590 Diepenbeek, Belgium

³IEMN, CNRS 8520, Bd Poincaré, Villeneuve d'Ascq 59651, France

(Received 11 July 2008; accepted 25 September 2008; published online 21 October 2008)

Hybrid giant magnetostrictive-piezoelectric film/film structures exhibiting magnetoelectric (ME) effect associated with a magnetic instability of the spin reorientation transition type are presented. We first present the theoretical study of a clamped beam actuator composed of a piezoelectric layer on a substrate actuated by a magnetostrictive layer. The actuator is a polished 50 μm thick 18 \times 5 mm^2 silicon substrate coated by an electrode, aluminum nitride, and magnetostrictive nanostructured layer. A ME coefficient of 30 $\text{V Oe}^{-1} \text{cm}^{-1}$ at a 35 KHz longitudinal resonance was measured. Nonlinear excitation of this mode showed a “nonlinear” dynamic ME coefficient of 4 $\text{V Oe}^{-1} \text{cm}^{-1}$. © 2008 American Institute of Physics. [DOI: 10.1063/1.3001601]

The magnetoelectric (ME) effect, predicted by P. Curie in 1894, is the change in electric polarization as a response to an applied magnetic field.^{1,2} With the development of techniques, the interest for these materials grew again (see Fiebig's reviews^{3,4}). “Stress mediated” composite materials mainly associating magnetostrictive and piezoelectric or electrostrictive based materials were created and displayed ME effects several orders of magnitude higher than natural ME materials. ME coefficient values as high as 10 $\text{V Oe}^{-1} \text{cm}^{-1}$ could be obtained in Terfenol-D/PMN-PT laminate composites. Higher values can be found in the case of resonant devices.^{5–8} Although they show interesting characteristics, most of these composites are still bulk materials and therefore hard to integrate in Micro-Electro-Mechanical-Systems or microelectronic devices. Recent works on ME epitaxial nanostructures showed very promising features.⁹ In the present work, we investigated rf-sputtered thin film based solutions combined with the use of a magnetic instability, which highly increases the sensitivity of the magnetomechanical interaction.¹⁰

In our previous work published in Ref. 11, with the configuration given in Fig. 1, we expressed the ME voltage amplitude for a given vibration mode n in the case of displacements along the z axis. It could be calculated that for the film/film ME layer on a thicker substrate, bending vibration modes can result in ME voltage, whereas torsion vibration will result in no amplitude. This model does not cover the case of vibrations occurring in the plane of the actuator. For the same geometry, we consider this time a longitudinal vibration mode. If U^n is the vibration envelope for the vibration mode n , the components of the displacement vector are U_x^n , U_y^n , and U_z^n . Contrary to the previous model, for the in plane vibrations we assume that $U_z^n=0$. One can then write the magnetoelastic free energy as $F_{\text{me}}^z = d_m B \mu_n \chi h A_n$. B is the magnetomechanical coupling constant, h is the magnetic excitation field, $\chi = \partial \varphi / \partial h$ is the magnetization angle susceptibility, and A_n is the amplitude of the considered mode. μ_n is

the magnetostrictive form factor that depends on the configuration of the actuator and the envelope U^n of the considered vibration mode. For longitudinal modes, $\mu_n = \int dS (\partial U_x^n / \partial x - \partial U_y^n / \partial y)$. In the longitudinal configuration, the piezoelectric energy is $F_p = -d_p E_3 (e_{31} - e_{33} C_{12} / C_{11}) \gamma_n A_n$. The e_{ij} are the piezoelectric coupling coefficients and C_{ij} are the elastic coefficients. Similar to μ_n , γ_n is the piezoelectric form factor and $\gamma_n = \int dS (\partial U_x^n / \partial x + \partial U_y^n / \partial y)$. The equation of motion is

$$\frac{\partial^2 A_n}{\partial t^2} + 2 \delta_n \dot{A}_n + \omega_n^2 A_n + \frac{1}{M_n} \frac{\partial}{\partial A_n} (F_{\text{me}} + F_p) = 0,$$

with the effective mass being $M_n = \rho d \int dS (U_x^2 + U_y^2)$. δ_n is the damping coefficient, ω is the pulsation, and ρ is the substrate density. The surface charge is given by $Q = \int D_3 dS$ and $V = E_3 d_p$ with the electrical displacement

$$D_3 = \varepsilon E_3 + (e_{31} - e_{33} C_{12} / C_{11}) \left(\frac{\partial U_x^n}{\partial x} + \frac{\partial U_y^n}{\partial y} \right) A_n,$$

where ε is the dielectric coefficient of the piezoelectric layer.

If no current is flowing, $\partial Q / \partial t = 0$ implies that $V = -d_p / \varepsilon S (e_{31} - e_{33} C_{12} / C_{11}) \gamma_n A_n$. The amplitude A_n is given by

$$A_n = \frac{-d_m B \mu_n \chi}{M_n (\Omega_n^2 - \omega^2 + 2i \delta_n \omega)} h,$$

with the renormalized frequency

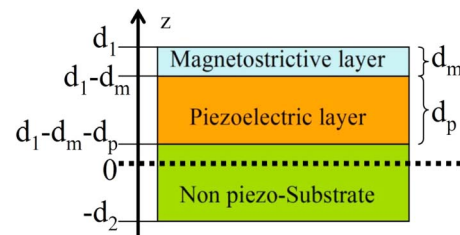


FIG. 1. (Color online) Side schematic view of the considered magnetostrictive actuator with integrated piezoelectric material.

^{a)}Electronic mail: nicolas.tiercelin@iemn.univ-lille1.fr.

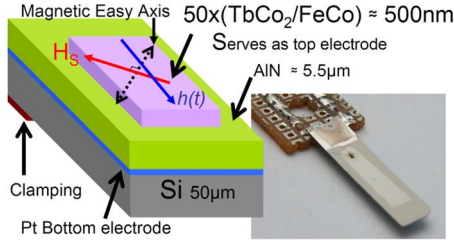


FIG. 2. (Color online) Left: magnetic field configuration for the clamped silicon beam coated with the AlN and the magnetostrictive layer. H_S is the polarizing field. $h(t)$ is the excitation field. Right: actual device.

$$\Omega_n^2 = \omega_n^2 + \frac{\gamma_n^2}{\varepsilon S M_n} d_p (e_{31} - e_{33} C_{12}/C_{11})^2.$$

Noting $f_n = \mu_n \gamma_n / S f(U_x^m + U_y^m) dS$, we obtain

$$V = \frac{d_m d_p B (e_{31} - e_{33} C_{12}/C_{11})^2}{d \varepsilon \rho} \frac{f_n}{(\Omega_n^2 - \omega^2 + 2i\delta_n \omega)} \chi h$$

being the amplitude of the generated ME voltage. This time, it shows that in this configuration, the ME generation is dictated by the compatibility of the form factors.

In our experiments, the considered device is a polished 50 μm thick 18 × 3 mm² silicon <100> substrate, on which a platinum electrode is deposited, and subsequently coated with aluminum nitride (AlN) followed by a giant magnetostrictive nanostructured layer, both deposited by rf sputtering. Piezoelectric AlN films were deposited by reactive dc-pulsed magnetron sputtering.¹² Pure aluminum is sputtered in a mixture of 50% argon and 50% nitrogen. The gases' flow rates are controlled by two mass flow meters, and the total gas flow rate is kept constant at 50 SCCM (SCCM denotes standard cubic centimeter per minute at STP). The distance between the target and the copper substrate holder is 5 cm. The substrates are not heated and their temperature is only dependent on the plasma heating. The base pressure is below 2 × 10⁻⁴ Pa. The target power supply is driven in constant-power mode at 600 W with a 250 kHz pulse frequency and 1600 ns pulse width. Before deposition, the target is cleaned in an argon discharge for 10 min and it is presputtered for additional 10 min. During these steps, the substrates are shielded from deposition by a shutter. Smooth, polycrystalline, and low stress AlN films with (002) texture (i.e., with the *c* axis perpendicular to the substrate) and a columnar structure are obtained. Prior to magnetic material deposition, in order to avoid short circuits, a resist was manually laid along the edges of the substrate. The giant nanostructured magnetostrictive film composed of 50 bilayers of TbCo₂(5 nm)/FeCo(5 nm) was subsequently deposited by rf sputtering. The magnetoelastic coupling coefficient, measured via the bending cantilever method¹³ on a test sample, was found to be $b\gamma^2 \approx -7$ MPa. A magnetic easy axis (EA) is obtained in the magnetic layer by applying a magnetic field during deposition. After removing the resist on the edges, this layer also serves as top electrode.

Figure 2 shows the considered device along with the magnetic field configuration used in the experiments. Previous works on magnetostrictive thin film actuators showed the possibility of a large sensitivity increase in the magnetomechanical coupling when using the properties of a field induced magnetic instability of the spin reorientation transition

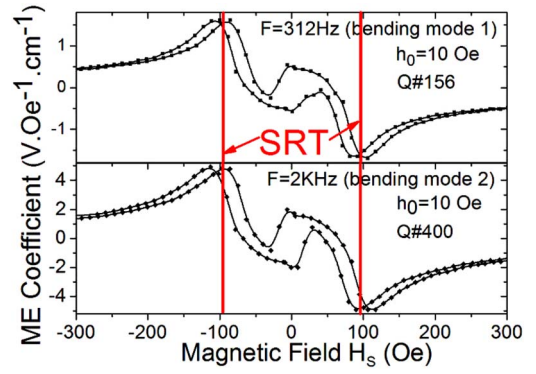


FIG. 3. (Color online) ME voltage for the first and second bending modes as a function of the polarizing field H_S .

(SRT) type. In order to induce the SRT in the magnetostrictive film, a polarizing field H_S is applied in the direction perpendicular to the magnetic EA of the film. The SRT is reached for H_S equal to the anisotropy field of the layer H_A , where the Zeeman interaction compensates the anisotropy, thus enabling a high sensitivity of magnetic moment to the driving field applied along the EA.^{14,15} For symmetry reasons, in this configuration, the favored excited vibration is the bending vibration as opposed to torsion.¹⁵ The compressive stress generated in the plane will also lead to in plane longitudinal vibration modes at higher excitation frequencies.

For the characterizations, an electromagnet is used to apply the SRT polarizing field H_S , and the alternative driving field $h(t)$ for the actuator is a 300 windings coil. The ME voltage picked between the bottom and the top electrode of the AlN layer is fed to a digital oscilloscope through a high impedance charge amplifier (voltage amplification equal to 1). The bending and torsion vibration amplitudes of the cantilever are recorded using a similar method as in Ref. 13. A two-dimensional position sensitive diode measures the deflection of a laser beam reflected on the tip of the cantilever. Quality factors of the resonance modes were determined using the amplitude versus frequency curves. The vibration spectrum of the actuator is fairly similar to what can be expected for a perfectly clamped cantilever. AlN has an elastic modulus of about 300 GPa (depending on the preparations conditions), whereas for Si it is about 170 GPa. Knowing that the silicon substrate is ten times thicker than the AlN layer and 100 times thicker than the magnetostrictive layer, the dynamic behavior of the clamped beam is mainly defined by the substrate.

Figure 3 shows the ME voltage amplitude measured as a function of the magnetic polarizing field H_S , when exciting the actuator at 321 and 2000 Hz, with a $h_0 = 10$ Oe (1 mT) magnetic field amplitude. Using the optical detection part of the experimental setup, these modes have been identified, respectively, as the first and second bending modes the actuator. For these modes and this geometry, the magnetostrictive and piezoelectric form factors¹¹ μ_1 , μ_2 , γ_1 , and γ_2 calculated with the analytical expression of the vibration deformation define f_1 as approximately equal to 0.21 and f_2 equal to 2.68. They are not equal to zero; thus these vibration modes are compatible with the ME generation. The effect of the SRT can be clearly seen in Fig. 3. When H_S reaches the anisotropy field value of the magnetic layer, the SRT takes place, magnetoelastic efficiency is enhanced, and so is the

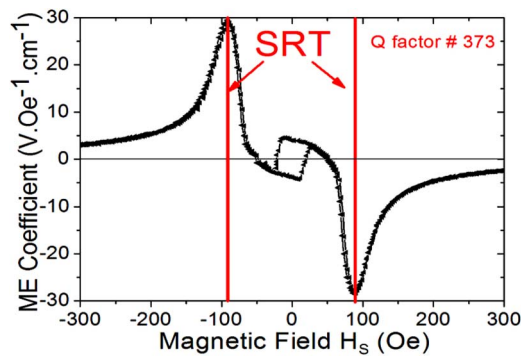


FIG. 4. (Color online) ME voltage for the first longitudinal mode as a function of the polarizing field H_S .

ME coefficient. The offset between the SRT points and the behavior around $H_S=0$ are due to the hysteretic nature of the magnetic layer. Using the SRT, a $1.5 \text{ V Oe}^{-1} \text{ cm}^{-1}$ value could be achieved with the first bending resonance mode and $4.8 \text{ V Oe}^{-1} \text{ cm}^{-1}$ with the second bending mode. Here, lower vibration amplitudes are compensated by higher Q and f coefficient. These values are obtained for a 500 nm active magnetic layer being 11 times thinner than the AlN layer.

Figure 4 shows the ME voltage amplitude measured as a function of the magnetic polarizing field H_S , when exciting the actuator at a frequency of 35 090 Hz with a 12.5 Oe (1.25 mT) magnetic field amplitude. This mode has been identified as the first longitudinal mode of the actuator. No bending or torsion angle could be measured optically. The effect of the SRT can also be clearly seen here. $30 \text{ V Oe}^{-1} \text{ cm}^{-1}$ could be achieved in resonant mode with a Q factor measured at 373. Again, the 500 nm active magnetic layer is 11 times thinner than the AlN layer. This high ME coefficient is due to a better efficiency of this vibration mode compared to bending modes: pure compressive or tensile stresses arise inside the piezolayer leading to a higher voltage through the d_{31} coefficient.

Finally, an SRT specific excitation mode was evidenced in this ME component: the “subharmonic” excitation already evidenced in nanostructured giant magnetostrictive thin films.¹⁶ Figure 5 shows the evolution of the ME voltage amplitude at 35 090 Hz, when the excitation field frequency is 17 545 Hz, with a 12.5 Oe (1.25 mT) amplitude. At the SRT point the “nonlinear” ME voltage amplitude can reach the value of $4 \text{ V Oe}^{-1} \text{ cm}^{-1}$, which is comparable to the value obtained for a direct excitation of the first bending modes. This feature is particularly useful for the design of high resonance frequency ME devices that can be excited by lower frequencies.

Thus, the ME effect in the $\text{AlN}/(\text{TbCo}_2/\text{FeCo}) \times \text{N}$ structures is enhanced using the properties of the field induced SRT in the magnetostrictive nanostructured film.

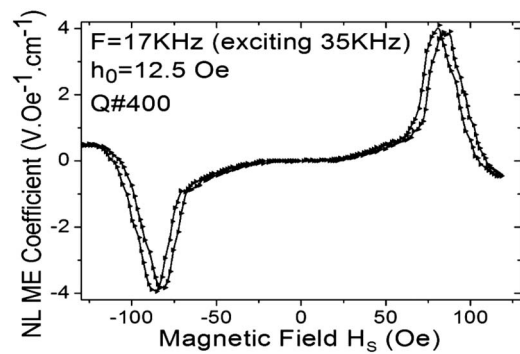


FIG. 5. ME voltage for the first longitudinal mode excited by half its frequency as a function of the polarizing field H_S .

$30 \text{ V Oe}^{-1} \text{ cm}^{-1}$ could be achieved in resonant mode, and a $4 \text{ V Oe}^{-1} \text{ cm}^{-1}$ nonlinear ME coefficient was measured. Applications are thought of in the microsystems domain. These results bring possibilities and tools for the design of integrated detection of vibrations in magnetostrictive actuators as well as high sensitivity ME magnetic field sensors.

This work was supported by the European project Inter-reg IIIa No.198 and the Russian State (Contract No. 02.513.11.3357).

¹P. Curie, *J. Phys. Theor. Appl.* **3**, 393 (1894).

²L. D. Landau and E. M. Lifshitz, *Electrodynamics of Continuous Media* (Pergamon, Oxford 1960), p. 119; Translation of Russian, *Electrodynamics of Continuous Media* (Pergamon, Oxford, 1958).

³M. Fiebig, *J. Phys. D* **38**, R123 (2005).

⁴N. A. Spaldin and M. Fiebig, *Science* **309**, 391 (2005).

⁵S. Dong, J. F. Li, and D. Viehland, *Appl. Phys. Lett.* **84**, 4188 (2004).

⁶J. G. Wan, Z. Y. Li, Y. Wang, M. Zeng, G. H. Wang, and J. Liu, *Appl. Phys. Lett.* **86**, 202504 (2005).

⁷H. Yu, M. Zeng, Y. Wang, J. G. Wan, and J. Liu, *Appl. Phys. Lett.* **86**, 032508 (2005).

⁸S. S. Guo, S. G. Lu, Z. Xu, X. Z. Zhao, and S. W. Or, *Appl. Phys. Lett.* **88**, 182906 (2006).

⁹H. Zheng, J. Wang, S. E. Lofland, Z. Ma, L. Mohaddes-Ardabili, T. Zhao, L. Salamanca-Riba, S. R. Shinde, S. B. Ogale, F. Bai, D. Viehland, Y. Jia, D. G. Schlom, M. Wuttig, A. Roytburd, and R. Ramesh, *Science* **303**, 661 (2004).

¹⁰N. Tiercelin, J. Ben Youssef, V. Preobrazhensky, P. Pernod, and H. Le Gall, *J. Magn. Magn. Mater.* **210**, 302 (2000).

¹¹N. Tiercelin, V. Preobrazhensky, P. Pernod, and A. Ostaschenko, *Appl. Phys. Lett.* **92**, 062904 (2008).

¹²V. Mortet, O. Elmazria, M. Nesladek, M. B. Assouar, G. Vanhoyland, J. D’Haen, M. D’Olieslaeger, and P. Alnot, *Appl. Phys. Lett.* **81**, 1720 (2002).

¹³E. du Trémolet de Lacheisserie and J. C. Peuzin, *J. Magn. Magn. Mater.* **136**, 189 (1994).

¹⁴N. Tiercelin, J. Ben Youssef, V. Preobrazhensky, P. Pernod, and H. Le Gall, *J. Magn. Magn. Mater.* **249**, 519 (2002).

¹⁵J. B. Youssef, N. Tiercelin, F. Petit, H. Le Gall, V. Preobrazhensky, and P. Pernod, *IEEE Trans. Magn.* **38**, 2817 (2002).

¹⁶N. Tiercelin, P. Pernod, V. Preobrazhensky, H. Le Gall, and B. Youssef, *Ultrasonics* **38**, 64 (2000).